


Investigation of Structural and Antimicrobial Properties of α -Fe₂O₃ Nanoparticles Synthesized by *Glycyrrhiza glabra* Plant Stem Extract

Shantinath Latthe¹, Suresh Kumbar², Sameer Kulkarni³, Suneel Dodamani¹,
Shidaling Matteppanavar^{4,*} 

¹ Dr. Prabhakar Kore Basic Science Research Centre, KLE Academy of Higher Education and Research, Belagavi, Karnataka, India-590010

² Department of Chemistry, KLE College of Engineering and Technology, Chikodi, Karnataka, India - 591201

³ Department of Physics, SKE Society's Govindram Seksaria Science College, Belagavi, Karnataka, India – 590003

⁴ Department of Physics, KLE Society's Basavaprabhu Kore Arts, Science and Commerce College, Chikodi, Karnataka, India - 591201

* Correspondence: siddutifr@gmail.com;

Received: 7.08.2024; Accepted: 12.07.2025; Published: 20.12.2025

Abstract: In this study, we have explored a green synthetic method using *Glycyrrhiza glabra* plant stem extract to prepare α -Fe₂O₃ nanoparticles. The X-ray diffraction analysis revealed a crystalline structure with broad peaks, indicating a rhombohedral structure with a centered hexagonal unit cell. Fourier transform infrared studies provided insights into Fe–O stretching vibration modes and confirmed that the synthesized nanoparticles are α -Fe₂O₃. UV-Visible absorption spectroscopy was performed, and the band gap of 2.4 eV was determined using the Tauc relation. Furthermore, the synthesized nanoparticles exhibited dose-dependent antibacterial activity against both Gram-negative and Gram-positive bacteria, as shown in the agar-well diffusion method. This research highlights the potential of green synthesis methods utilizing plant extracts for the fabrication of functional nanoparticles with promising antibacterial properties.

Keywords: α -Fe₂O₃ nanoparticles; green method; structure; antimicrobial.

© 2025 by the authors. This article is an open-access article distributed under the terms and conditions of the Creative Commons Attribution (CC BY) license (<https://creativecommons.org/licenses/by/4.0/>), which permits unrestricted use, distribution, and reproduction in any medium, provided the original work is properly cited. The authors retain copyright of their work, and no permission is required from the authors or the publisher to reuse or distribute this article, as long as proper attribution is given to the original source.

1. Introduction

Metal oxide nanoparticles have gathered significant attention in recent years due to their distinctive optical, magnetic, and electronic properties. These nanomaterials exhibit novel characteristics compared to their bulk counterparts, largely attributed to their reduced size and increased surface area [1-3]. These features have the potential to deliver exceptional performance across various domains, including catalysis, magnetism, mechanics, and biology. Among these nanoparticles, Magnetite nanoparticles (MNPs) are widely explored in the biomedical field due to their biocompatibility, chemical stability, and magnetic properties [4]. α -Fe₂O₃ transition-metal oxide nanoparticles have been widely studied and find applications in various fields. Its unique properties make it suitable for a range of technological and biological applications like catalysts, sensors, ceramics, data storage materials and dyes, drug delivery, magnetic resonance imaging, and bioremediation [5-8].

The green synthesis of nanoscale Fe₂O₃ using plant extracts such as *Hordeum vulgare* (barley) [9], *Rumex acetosa* (common sorrel) [9], and *Azadirachta indica* (neem) [10] has attracted significant attention from researchers in recent years. This approach uses the reducing and stabilizing agents present in plant extracts to synthesize iron oxide nanoparticles. Green synthesis approaches are preferred over conventional chemical reduction methods due to their eco-friendliness and lower toxicity. Employing plant extracts as reducing agents reduces the need for hazardous chemicals, making the synthesis process more environmentally benign [11]. Fe₂O₃ nanoparticles are widely recognized as effective photocatalysts [12,13], as demonstrated by their ability to facilitate the photo-degradation of detrimental industrial pollutants, including dyes [14]. Extensive investigations have been conducted on the anticancer properties of Fe₂O₃ nanomaterials, driven by their potential utility in targeted drug delivery systems and magnetic hyperthermia therapy for cancer treatment [15].

This study describes the biological synthesis of α -Fe₂O₃ using *Glycyrrhiza glabra* plant stem extract as a reducing or stabilizing agent for nanoparticle formation. *Glycyrrhiza glabra*, also known as the 'Grandfather of the herb' or sweet wood (*Glycyrrhiza glabra*), originates from Asia, Southern Europe, and North Africa. Conventionally, it has been incorporated into various medicinal formulations for its roles as a sweetener, expectorant, antitussive, demulcent, and purgative. In eastern cultures, the dried rhizome and roots of *Glycyrrhiza glabra* have been recognized as essential medicinal components. In contemporary times, extracts of *Glycyrrhiza glabra* are commonly used as flavouring agents in formulations to mask the unpleasant taste of cold and cough preparations. Additionally, its anti-inflammatory activity contributes to liver conditioning, and it is extensively utilized in addressing ailments such as arthritis and mouth ulcers to alleviate pain [16,17]. In Japan, Licorice extracts are employed for the treatment of various virus-borne infections. The combination of *Glycyrrhiza glabra* extracts with other drugs has been found to be beneficial for conditions such as psoriasis and herpetic lesions, as it helps soothe and heal skin eruptions [18]. Recently, Vinayagam *et al.* reported the green synthesis of nanoscale α -Fe₂O₃ nanoparticles using the leaf extract of *Spondias dulcis* [19]. Biswal *et al.* synthesised the Ag-doped Fe₂O₃ nanocomposite using *Psidium guajava* extract and developed an environmentally friendly, renewable adsorbent for the remediation of Cr(VI) from aqueous solution [20]. Green synthesis of iron oxide nanoparticles using *Rheum emodi* and their antimicrobial and anticancer effects in vitro, reported by Sharama *et al.* [21]. Mbachu *et al.* reported on iron oxide (α -Fe₂O₃) nanoparticles synthesized using Taguchi extract and explored their biomedical prospects [22]. Jasrotia *et al.* report the pure Ag, Cu, and Fe₂O₃ nanoparticles [23]. Karpagavinayagam *et al.* designed the Fe₂O₃ nanoparticles using *Avicennia marina* flower extract [24]. Freire *et al.* biosynthesis of iron oxide nanoparticles using *Caesalpinia coriaria* (Jacq.) Wild. fruit extract [25].

Glycyrrhiza glabra root has a long history of use in Chinese medicine, spanning more than a millennium. Its medicinal effects are attributed to a diverse array of active compounds, including isoflavonoids, chalcones, amino acids, lignins, amines, gums, and volatile oils. Research has identified over 20 triterpenoids and 300 flavonoids within its structure, highlighting its rich chemical diversity and making it a compelling subject for scientific investigation. The *Glycyrrhiza glabra* (licorice) plant stem extract used for the synthesis of high-quality α -Fe₂O₃ (hematite) nanoparticles is based on several key factors. *Glycyrrhiza glabra* contains a variety of phytochemicals, including flavonoids, saponins, and glycyrrhizin, which can act as reducing and stabilizing agents in the synthesis of nanoparticles. These compounds can facilitate the reduction of iron ions to form α -Fe₂O₃ while preventing

agglomeration. Also, phytochemicals, including flavonoids, saponins, and glycyrrhizin, functionalize the surface of the α -Fe₂O₃ nanoparticle, which is useful for various applications. Most importantly, this extract generally enhances biocompatibility, making the resulting nanoparticles more suitable for biomedical applications, such as drug delivery and imaging. Synthesis using plant extracts is a greener alternative to traditional chemical methods, which often involve toxic solvents and reducing agents. The use of natural materials aligns with sustainable practices. Plant extracts are typically abundant and inexpensive, making the synthesis process more economical compared to synthetic chemicals. Other plant extracts (such as those from Aloe vera, green tea, or neem) may also reduce iron ions, but their efficiency can vary depending on their specific phytochemical content and concentration. The efficacy of nanoparticle synthesis can be influenced by the type of active compounds present in the extract. The size and stability of nanoparticles can differ between extracts. Some plants may produce larger or more agglomerated nanoparticles, whereas *G. glabra*'s compounds might yield smaller, more uniform particles. Different plant extracts can impart unique functional properties to the nanoparticles. For example, some extracts may enhance antibacterial or antioxidant activities more than others, depending on their specific bioactive compounds.

Recently, the issue of multidrug resistance and extensive drug resistance to antibiotics has escalated to a critical point, necessitating immediate action [26]. This presents unprecedented dangers to both human and animal health in the twenty-first century. Moreover, the development of new antibiotics is declining due to high development costs and low returns on investment [27]. Inorganic nanoparticles with magnetic properties offer a promising approach for combating antibiotic-resistant bacteria, as they do not depend on targeting specific antibiotic resistance mechanisms [28]. PEG-coated Fe₃O₄ nanoparticles have shown notable effectiveness in both antimicrobial and anticancer activities [29]. Chitosan-pectin films embedded with Fe₃O₄ magnetic nanoparticles offer promising potential for advanced, intelligent food packaging solutions [30]. CoAF and CuAF nanocomposites hold significant promise as antibacterial agents for various biomedical applications [31]. Nanoparticles are also highly effective in various fields, including sensors, medical devices, drug delivery, antibacterial applications, dye degradation, and DNA labeling [32]. Nowadays, many treatment techniques, such as cancer diagnosis [33], adsorption [34], chemical precipitation [35], coagulation [36], advanced oxidation processes [37], and osmosis [38], have shown wide applications across different fields.

Overall, from the above detailed literature survey, it is necessary to explore α -Fe₂O₃ with different plant extracts due to its unique morphology, which plays a crucial role in antimicrobial studies and effects. In this study, we have successfully utilized an eco-friendly approach to synthesize α -Fe₂O₃ nanoparticles from *Glycyrrhiza glabra* plant stem extract. The synthesized nanoparticles were subjected to studies of their structure, optical, and antimicrobial properties. The resulting nanoparticles exhibit noteworthy antibacterial activity, demonstrating their potential for diverse applications in biomedical and materials science.

2. Materials and Methods

The *Glycyrrhiza glabra* plant stem is medically certified by KLE Ayurveda Medical College, Belgaum, India. Ferric chloride (FeCl₃) purchased from Sigma-Aldrich. All aqueous solutions were prepared in double-distilled water.

Thoroughly washed the procured *Glycyrrhiza glabra* plant stem with distilled water to remove dust particles and other impurities, to ensure that the extract is free from contaminants.

Finely chop 20 grams of the washed plant stem. The chopping process increases the surface area, facilitating efficient extraction. Added the finely chopped plant stem to 100 ml of deionized water and heated the mixture to 90°C, and maintained this temperature for 45 minutes. This process helps in extracting compounds from the plant stem into the water. After heating, allow the mixture to cool to room temperature. This step is crucial to avoid potential degradation of heat-sensitive compounds. Separated the extract from the solid plant material by filtration. Used Whatman filter paper no.4. This process removes any remaining solid particles, yielding a clear liquid extract. The pH of the extract is measured (Figure 1).

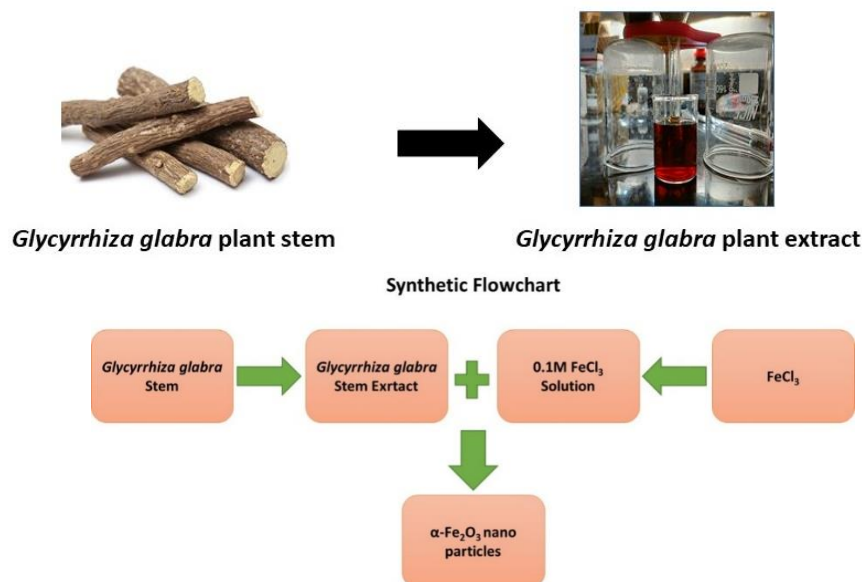


Figure 1. Preparation of *Glycyrrhiza glabra* plant stem extract and Flowchart.

5ml of the extract is added to the 20ml of 0.1M FeCl₃ solution, heated at 70°C for 10 minutes with constant stirring. The formation of the nanoparticles will be identified by a change in the solution's color to dark brown (Figure 2). The as-synthesized nanoparticles were centrifuged and rinsed with DI water 10-12 times to remove impurities, then dried for further studies.

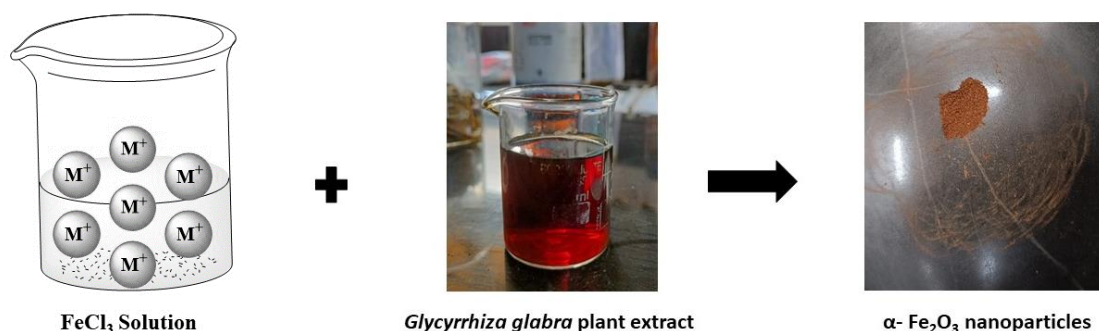


Figure 2. Synthesis of Fe₂O₃ nanoparticles.

3. Results and Discussion

Figure 3 depicts the X-ray diffraction (XRD) patterns of as synthesized α-Fe₂O₃ nano particles, which shows the low intense diffraction humps with broadening nature. After careful analysis, small humps are noticed and it is well matching with the α-Fe₂O₃ phase (JCPDS-ICDD card number 89-0596) [39]. The matched JCPDS card shows the rhombohedral structure with a centered hexagonal structure (R-3c space group) (JCPDS-ICDD card number 89-0596)

[26]. The annealed XRD pattern exhibits the selected main characteristic peaks at different 2θ values of 24.1° , 33.2° , 35.6° , 49.5° , and 54.1° , corresponding to the hkl planes (012), (104), (110), (113), and (024), respectively.

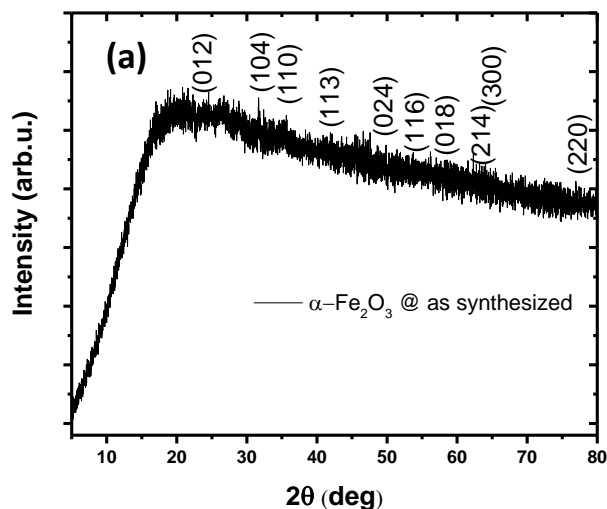


Figure 3. XRD pattern of as-synthesized α - Fe_2O_3 nanoparticles.

The particle size and macrostrain were estimated using the Debye-Scherrer formula, yielding 40.75 nm and 0.82 nm, respectively. The obtained Bond distance and Bond angle are $\text{Fe-O} = 2.126$ (5) Å, $\text{Fe-Fe} = 0.666$ (2) Å, respectively. The observation of low-intensity diffraction humps with broadening in X-ray diffraction (XRD) patterns typically indicates several important characteristics about the material being studied. Here's a detailed interpretation of these results and possible causes of the broadening. Low-intensity peaks suggest that the material may have limited crystallinity or a small amount of crystalline phase. This can occur in amorphous materials or in materials with small crystallite sizes. The presence of humps rather than sharp peaks may indicate a mixture of phases or amorphous content in the sample. If there are multiple phases, their overlapping peaks can lead to broad humps. The broadening can also hint at microstructural features, such as strain or defects within the crystal lattice, which can affect the positions and intensities of diffraction peaks.

Broadening of XRD data can be used to estimate crystallite size; according to the Scherrer equation, smaller crystallite sizes lead to broader peaks. This is often observed in nanomaterials where the crystallite size is reduced to the nanoscale. Internal stress or strain in the material can lead to peak broadening. Strain can arise from defects, phase changes, or during processing (e.g., during synthesis or thermal treatment). Some broadening can be attributed to the instrumental setup used for the XRD measurement. However, this is usually accounted for in data analysis, and the intrinsic broadening of the sample is primarily considered. Elevated temperatures during measurement can increase atomic vibrations (Debye-Waller effect), thereby contributing to peak broadening. If a significant portion of the sample is amorphous, the XRD pattern may show broad features instead of sharp peaks. This is common in certain materials like glasses or polymers. The combination of low-intensity, broad diffraction humps suggests a material that may be nanocrystalline, contain structural defects, or be partially amorphous. Quantitatively analyzing the degree of broadening (using the Scherrer equation or a Williamson-Hall plot) can provide insights into the crystallite size and strain in the material.

Figure 4 shows the arrangement of Fe (red color) and O (yellow color) in a distorted Hexagonal structure. In general, α - Fe_2O_3 hematite crystallizes in a corundum structure. It is

well categorized by a faintly distorted hexagonal close-packed oxide-ion lattice where 2/3 of the octahedral sites are occupied by Fe³⁺ ions with nondegenerated energy levels on metal d-electrons because of ligand field splitting created from Fe-O hybridization (Figure 4) [40]. Oxygen ions that are situated parallel to (0001) planes are detached by an iron double layer, resulting in a tacking sequence of O₃-Fe-Fe repeat units [40].

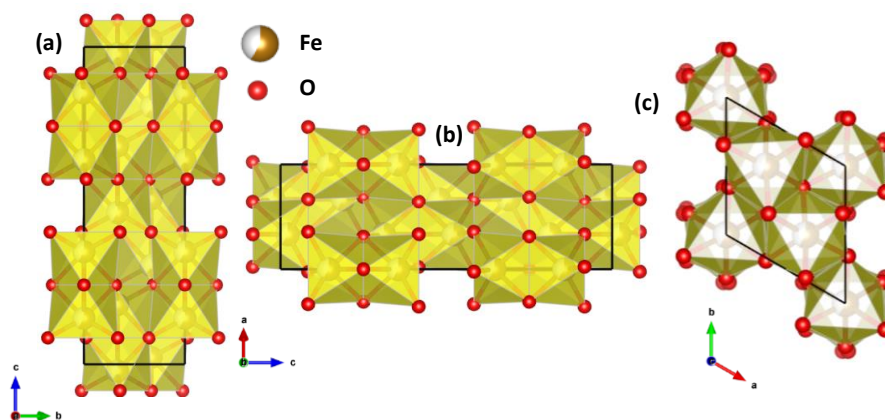


Figure 4. Polyhedral structure of α -Fe₂O₃ at different directions along (a) a; (b) b ;(c) c-axis.

Figure 5 shows the FTIR spectra of α -Fe₂O₃ nanoparticles of infrared absorption properties through the stretching and bending vibrations. From the data, we have identified 6 prominent peaks, which are consistent with the stretching and bending vibrations of α -Fe₂O₃ nanoparticles. The bands at 423, 447, 472, and 508 cm⁻¹ indicate the presence of Fe–O stretching vibration modes. This clearly confirms that the synthesized nanoparticles are α -Fe₂O₃, and it is well corroborated by the XRD data in Figure 3. The absorption peaks are observed around 1026 and 1599 cm⁻¹ [41]. These modes can be assigned to the stretching and bending vibrations of OH groups of H₂O molecules [42–45]. The slight difference between the modes in the presented and reported data is due to differences in morphology and synthesis conditions [42, 43, 46, 47]. The correlation between FTIR spectra showing Fe–O stretching vibrations and XRD data for α -Fe₂O₃ nanoparticles can provide valuable insights into the material's structural characteristics. In FTIR spectroscopy, peaks corresponding to Fe–O stretching vibrations are indicative of the presence of iron oxide, specifically α -Fe₂O₃ (hematite). These peaks typically appear in the range of approximately 400–600 cm⁻¹. The intensity and position of these peaks can provide information about the bonding environment of the iron ions within the structure. XRD data provides information on the crystalline structure of the nanoparticles. If the FTIR peaks align with the expected wavenumbers for Fe–O vibrations in α -Fe₂O₃, and the XRD patterns show peaks corresponding to this phase, it supports the conclusion that the nanoparticles are indeed α -Fe₂O₃. The intensity of the FTIR peaks can correlate with the crystallinity indicated by XRD. Strong, sharp peaks in XRD suggest a highly crystalline material, which may also enhance the intensity of the FTIR features due to more ordered bonding environments. Variations in peak positions or intensities in FTIR could hint at size effects or morphological deviations, which might be corroborated by XRD data showing broader peaks (indicative of smaller particle sizes or strain) or different peak intensities. Overall, the combination of FTIR and XRD results provides a comprehensive understanding of the structural and bonding characteristics of α -Fe₂O₃ nanoparticles. Confirming both the presence of Fe–O bonds via FTIR and the crystalline structure via XRD reinforces the validity of your characterization and helps elucidate the properties relevant to applications in catalysis, sensors, and other fields.

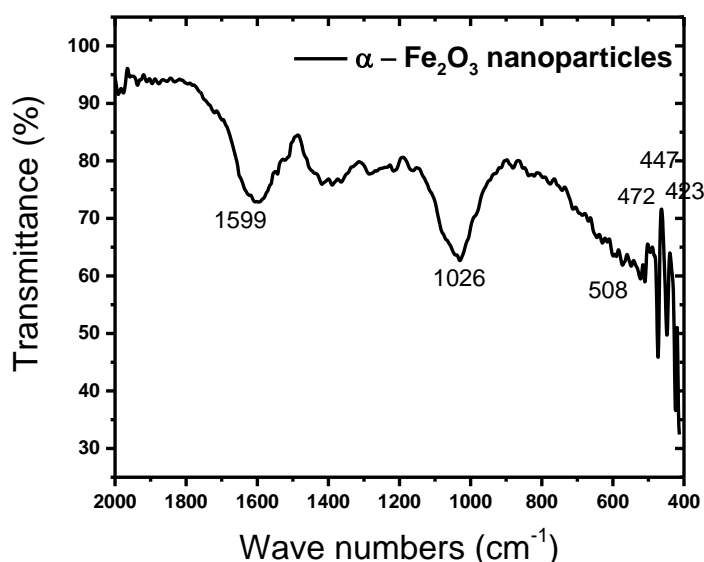


Figure 5. FTIR spectra of α -Fe₂O₃ nanoparticles show infrared absorption properties through the stretching and bending vibrations.

During the absorption of electromagnetic waves, electrons are excited from the highest occupied molecular orbital (HOMO) in the valence band to the lowest unoccupied molecular orbital (LUMO) in the conduction band. The band gap energy of the material is determined by the wavelength of light absorbed in transitions between bonding and antibonding orbitals. Optical absorbance of α -Fe₂O₃ nanoparticles was measured at room temperature using a JASCO UV-Visible spectrophotometer, with a focus on the 200-800 nm wavelength range. The obtained spectrum is depicted in Figure 6a. A prominent absorption peak is observed in the vicinity of the visible region, approximately at 300 nm. The band gap energy of α -Fe₂O₃ nanoparticles was determined through the application of the Tauc relation.

$$(\alpha h\nu)^n = C(h\nu - E_g) \quad (1)$$

Where α is the absorption coefficient, h is Planck's constant, ν is the frequency of vibration, C is the proportionality constant, E_g is the average band gap energy, and the value of n depends on the type of transition. The Tauc relation provides a direct and effective method for analyzing optical absorption data, allowing us to estimate the band gap energy from the absorption spectrum quickly. This is particularly advantageous when working with complex materials where more sophisticated methods may not be feasible. Typically, a Tauc plot shows $h\nu$ (the photon energy) on the abscissa (x-axis) and $(\alpha h\nu)^{1/2}$ on the ordinate (y-axis), where α is the material's absorption coefficient. Thus, extrapolating the linear region to the abscissa yields the optical bandgap energy of the amorphous material. Figure 6b illustrates the Tauc plot; the band gap energy derived from the Tauc plot is 2.4 eV. This value exceeds the reported band gap energy for the majority-carrier hematite. The difference is due to quantum confinement, which affects the delocalization of electronic states near the Fermi level [48-50].

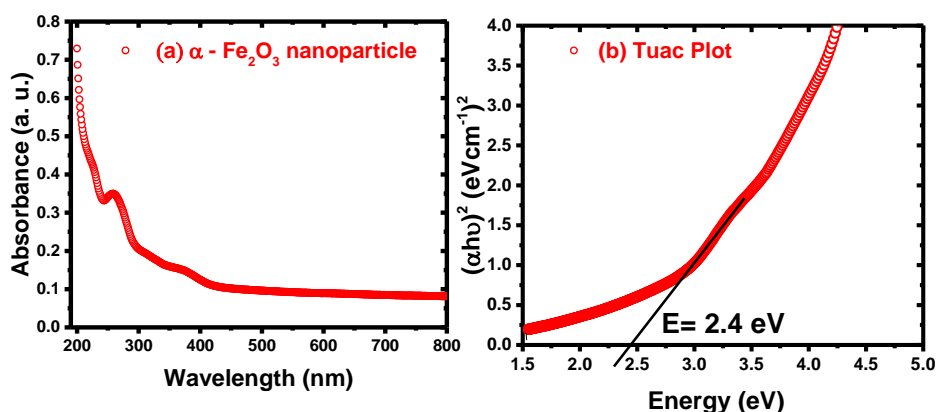


Figure 6. UV-Visible absorption spectrum and Tauc plot of α -Fe₂O₃ nanoparticles.

TEM was used to determine the exact particle size of the synthesized α -Fe₂O₃. The particle size of the prepared nanoparticles was found to be around 50 nm. It is well matched with the particle size obtained by the Debye-Scherrer method. Also, it is depicted as an asymmetric morphology with uniform dispersion during hematite phase formation (Figure 7).

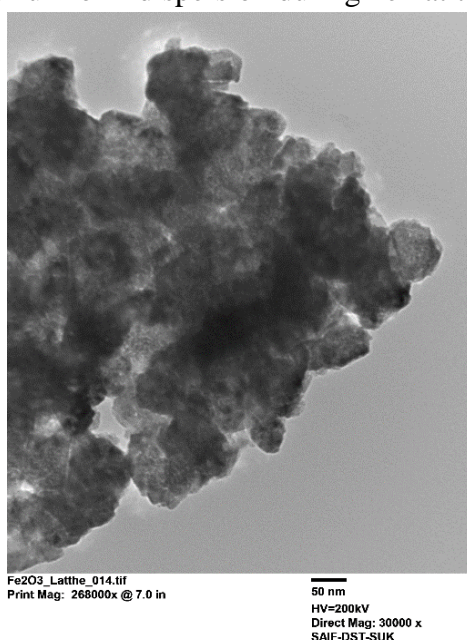


Figure 7. Transmission electron microscopy image of α -Fe₂O₃ NPs.

3.1. *In vitro* anti-bacterial activity.

From the aforementioned facts, it is evident that compounds containing α -Fe₂O₃ exhibit potent biological activities. When the Fe₂O₃ system is fused or coupled with other hybrids, the resulting conjugates are expected to demonstrate enhanced biological properties. Hence, α -Fe₂O₃ has been synthesized. These composites have been screened for *in vitro* antibacterial activity.

The synthesized α -Fe₂O₃ nanoparticles were tested for their antibacterial screening with various concentrations against pathogenic bacterial strains, viz., *S. aureus* (ATCC 29413), *B. subtilis* (NCIB 8057), *B. cereus* (ATCC 11778), *C. botulinum* (ATCC 443), *E. coli* (ATCC 25992), *P. aeruginosa* (NCIB 8295), *K. pneumoniae* (ATCC 10031), and *S. typhi* (14028) through the disc diffusion method [51]. All incubations and tests were conducted in triplicate. In this experiment, ciprofloxacin was employed as the reference drug to compare antibacterial activities.

A 5% DMSO solution was utilized to dissolve the compounds, and the disc diffusion method was employed to determine antimicrobial activity by measuring the zone of inhibition. To elucidate the potential role of DMSO in biological screening, separate studies were conducted using solutions of DMSO alone, revealing no activity against any bacterial strains. The tests were carried out at 30, 60, and 90 $\mu\text{g mL}^{-1}$ concentrations. After 2 days of incubation at 37°C, the zone of inhibition was measured in mm. The investigation of antibacterial screening of $\alpha\text{-Fe}_2\text{O}_3$ against human pathogenic bacterial strains showed good to excellent inhibition compared with the reference drug. Screening results are summarized in Table 1.

Table 1. Summarized Screening results of human pathogenic bacterial strains against $\alpha\text{-Fe}_2\text{O}_3$.

Diameter of growth of inhibition zone (mm)

Concentration	<i>S. aureus</i> ATCC 29413	<i>B. subtilis</i> NCIB 8057	<i>B. cereus</i> ATCC 11778	<i>C. botulinum</i> ATCC 443	<i>E. coli</i> ATCC 25992	<i>P. aeruginosa</i> NCIB 8295	<i>K. pneumonia</i> ATCC 10031	<i>S. Typhi</i> 14028
30 μg	8.2 \pm 0.01	4.4 \pm 0.3	7.4 \pm 0.16	4.8 \pm 0.3	7.4 \pm 0.16	5.6 \pm 0.3	-	6.9 \pm 0.2
60 μg	12.2 \pm 0.0	9.8 \pm 0.2	11.6 \pm 0.1	6.2 \pm 0.05	12.3 \pm 0.3	10.1 \pm 0.5	-	12.3 \pm 0.6
90 μg	14.6 \pm 0.4	13.4 \pm 0.0	13.8 \pm 0.1	9.8 \pm 0.1	15.2 \pm 0.1	11.6 \pm 0.6	7.6 \pm 0.2	13.6\pm0.5
Controlciprofloxacin	19.5 \pm 0.0	19.6 \pm 0.3	20.3 \pm 1.2	12.6 \pm 0.5	20.2 \pm 0.0	18.0 \pm 0.3	24.3 \pm 0.1	20.0 \pm 0.6

Iron nanoparticles have shown significant activity against various cancer cell lines. Their cytotoxic effects are mainly attributed to the iron core itself, particularly before oxidation, rather than to the iron ions released from it. This unique property makes iron nanoparticles highly valuable for several applications, including drug delivery systems, diagnostic probes, and hyperthermia treatments. By harnessing their capabilities, researchers are exploring innovative ways to improve cancer therapies and enhance diagnostic accuracy. Another notable property of iron nanoparticles is their ability to selectively suppress the growth of cancer cells while leaving healthy cells largely unaffected, especially before oxidation occurs. This targeted action makes iron nanoparticles a promising therapeutic tool in nanomedicine. Their potential to minimize damage to healthy tissue while effectively targeting cancerous cells could lead to more effective, less harmful cancer treatments. Both *Glycyrrhiza glabra* and $\alpha\text{-Fe}_2\text{O}_3$ nanoparticles have a wide range of biomedical applications, demonstrating their versatility and potential to improve health outcomes.

4. Conclusions

In this present work, $\alpha\text{-Fe}_2\text{O}_3$ nanoparticles were synthesized by the green synthesis method using *Glycyrrhiza glabra* plant stem extract. It indicates that the *Glycyrrhiza glabra* plant stem extract can successfully produce high-quality polycrystalline $\alpha\text{-Fe}_2\text{O}_3$ nanoparticles. The particle size of the prepared nanoparticles is between 40 and 50 nm. The FTIR spectra of $\alpha\text{-Fe}_2\text{O}_3$ nanoparticles show the stretching and bending vibrations. From the data, 6 prominent peaks are observed, which corroborate the stretching and bending vibrations of $\alpha\text{-Fe}_2\text{O}_3$ nanoparticles. The absorption peaks are observed around 1026 and 1599 cm^{-1} ; these modes can be assigned to the stretching and bending vibrations of the OH groups of H_2O molecules. A prominent absorption peak is observed in the visible region, approximately at 300 nm, as measured by UV-Vis spectroscopy. The band gap derived from the Tauc plot is 2.4 eV. The particle size of the synthesized nanoparticles was found to be around 50 nm, which is well matched to the particle size obtained by the Debye-Scherrer method. The antimicrobial activity of the nanoparticles at different concentrations was tested against various bacteria. It exhibits good to excellent inhibition when compared to the reference drug.

Author Contributions

Conceptualization, S.L. and S.M.; methodology, S.L. and S.M.; investigation, S.K., S.K., and S.D.; formal analysis, S.K., S.K., and S.D.; writing—original draft preparation, S.L. and S.M.; writing—review and editing, all authors. All authors have read, discussed the results, and agreed to the published version of the manuscript.

Institutional Review Board Statement

Not applicable.

Informed Consent Statement

Not applicable.

Data Availability Statement

Data will be made available based on request.

Funding

Vision Group on Science and Technology for sanctioning the project under the "Centre of Excellence in Science, Engineering and Medicine" (CESEM GRD No 852), Government of Karnataka. UGC-DAE Consortium of Scientific Research letter/Order No. 2021-22/03/587 dated 30/03/2022 for the financial support.

Acknowledgments

SL and SM acknowledge the Vision Group on Science and Technology for sanctioning the project under the "Centre of Excellence in Science, Engineering and Medicine" (CESEM GRD No 852), Government of Karnataka. SM also thanks the UGC-DAE Consortium of Scientific Research, Letter/Order No. 2021-22/03/587 dated 30/03/2022, for the financial support. SL thanks the Directorate of Minorities, Government of Karnataka, for providing a PhD Fellowship.

Conflicts of Interest

The authors don't have any conflicts of interest.

References

1. Alivisatos, A.P. Semiconductor Clusters, Nanocrystals, and Quantum Dots. *Science* **1996**, *271*, 933-937, <https://doi.org/10.1126/science.271.5251.933>.
2. Klimov, V.I.; Mikhailovsky, A.; Xu, S.; Malko, A.; Hollingsworth, J.A.; Leatherdale, a.C.; Eisler, H.-J.; Bawendi, M. Optical gain and stimulated emission in nanocrystal quantum dots. *Science* **2000**, *290*, 314-317, <https://doi.org/10.1126/science.290.5490.314>.
3. Fernandez-Garcia, M.; Martinez-Arias, A.; Hanson, J.; Rodriguez, J. Nanostructured oxides in chemistry: characterization and properties. *Chem.Rev.* **2004**, *104*, 4063-4104, <https://doi.org/10.1021/cr030032f>.
4. Mahdavi, M.; Ahmad, M.B.; Haron, M.J.; Namvar, F.; Nadi, B.; Rahman, M.Z.A.; Amin, J. Synthesis, Surface Modification and Characterisation of Biocompatible Magnetic Iron Oxide Nanoparticles for Biomedical Applications. *Molecules* **2013**, *18*, 7533-7548, <https://doi.org/10.3390/molecules18077533>.

5. Cherepy, N.J.; Liston, D.B.; Lovejoy, J.A.; Deng, H.; Zhang, J.Z. Ultrafast studies of photoexcited electron dynamics in γ - and α -Fe₂O₃ semiconductor nanoparticles. *J. Phys. Chem.* **1998**, *102*, 770-776, <https://doi.org/10.1021/jp973149e>.
6. Chen, J.; Xu, L.; Li, W.; Gou, X. α -Fe₂O₃ Nanotubes in Gas Sensor and Lithium-Ion Battery Applications. *Advanced Materials* **2005**, *17*, 582-586, <https://doi.org/10.1002/adma.200401101>.
7. Tang, B.; Wang, G.; Zhuo, L.; Ge, J.; Cui, L. Facile route to α -FeOOH and α -Fe₂O₃ nanorods and magnetic property of α -Fe₂O₃ nanorods. *Inorg. Chem.* **2006**, *45*, 5196-5200, <https://doi.org/10.1021/ic060097b>.
8. Lindgren, T.; Wang, H.; Beermann, N.; Vayssieres, L.; Hagfeldt, A.; Lindquist, S.-E. Aqueous photoelectrochemistry of hematite nanorod array. *Sol. Energy Mater. Sol. Cells* **2002**, *71*, 231-243, [https://doi.org/10.1016/S0927-0248\(01\)00062-9](https://doi.org/10.1016/S0927-0248(01)00062-9).
9. Makarov, V.V.; Makarova, S.S.; Love, A.J.; Sinityna, O.V.; Dudnik, A.O.; Yaminsky, I.V.; Taliansky, M.E.; Kalinina, N.O. Biosynthesis of stable iron oxide nanoparticles in aqueous extracts of *Hordeum vulgare* and *Rumex acetosa* plants. *Langmuir* **2014**, *30*, 5982-5988, <https://pubs.acs.org/doi/abs/10.1021/la5011924>.
10. Sharma, J.K.; Srivastava, P.; Akhtar, M.S.; Singh, G.; Ameen, S. α -Fe₂O₃ hexagonal cones synthesized from the leaf extract of *Azadirachta indica* and its thermal catalytic activity. *New J. Chem.* **2015**, *39*, 7105-7111, <https://doi.org/10.1039/C5NJ01344E>.
11. Narayanan, K.B.; Sakthivel, N. Biological synthesis of metal nanoparticles by microbes. *Adv. Colloid Interface Sci.* **2010**, *156*, 1-13, <https://doi.org/10.1016/j.cis.2010.02.001>.
12. Apte, S.; Naik, S.; Sonawane, R.; Kale, B.; Baeg, J. Synthesis of nanosize-necked structure α - and γ -Fe₂O₃ and its photocatalytic activity. *J. Am. Ceram. Soc.* **2007**, *90*, 412-414, <https://doi.org/10.1111/j.1551-2916.2006.01424.x>.
13. Qu, X.; Kobayashi, N.; Komatsu, T. Solid nanotubes comprising α -Fe₂O₃ nanoparticles prepared from ferritin protein. *ACS Nano* **2010**, *4*, 1732-1738, <https://doi.org/10.1021/nn901879d>.
14. Zhou, X.; Yang, H.; Wang, C.; Mao, X.; Wang, Y.; Yang, Y.; Liu, G. Visible light induced photocatalytic degradation of rhodamine B on one-dimensional iron oxide particles. *J. Phys. Chem. C* **2010**, *114*, 17051-17061, <https://doi.org/10.1021/jp103816e>.
15. Sato, I.; Umemura, M.; Mitsudo, K.; Fukumura, H.; Kim, J.-H.; Hoshino, Y.; Nakashima, H.; Kioi, M.; Nakakaji, R.; Sato, M. Simultaneous hyperthermia-chemotherapy with controlled drug delivery using single-drug nanoparticles. *Sci. Rep.* **2016**, *6*, 24629, <https://doi.org/10.1038/srep24629>.
16. The Wealth of India: A Dictionary of Indian Raw Materials and Industrial Products (Industrial Products—Part I). *Ind. Med. Gaz.* **1949**, *84*, 476-477.
17. Fatima, A.; Gupta, V.K.; Luqman, S.; Negi, A.S.; Kumar, J.; Shanker, K.; Saikia, D.; Srivastava, S.; Darokar, M.; Khanuja, S.P. Antifungal activity of *Glycyrrhiza glabra* extracts and its active constituent glabridin. *Phytother. Res.* **2009**, *23*, 1190-1193, <https://doi.org/10.1002/ptr.2726>.
18. Aluckal, E.; Ismail, A.; Paulose, A.; Lakshmanan, S.; Balakrishnan, M.S.; Mathew, B.; Vikneshan, M.; Kunnilathu, A. Assessment of Total Antioxidant Capacity and Antimicrobial Activity of *Glycyrrhiza glabra* in Saliva of HIV-Infected Patients. *J. Pharm. Bioallied Sci.* **2017**, *9*, S237-s240, https://doi.org/10.4103/jpbs.jpbs_141_17.
19. Vinayagam, R.; Pai, S.; Varadavenkatesan, T.; Narasimhan, M.K.; Narayanasamy, S.; Selvaraj, R. Structural characterization of green synthesized α -Fe₂O₃ nanoparticles using the leaf extract of *Spondias dulcis*. *Surf. Interfaces* **2020**, *20*, 100618, <https://doi.org/10.1016/j.surf.2020.100618>.
20. Biswal, S.K.; Panigrahi, G.K.; Sahoo, S.K. Green synthesis of Fe₂O₃-Ag nanocomposite using *Psidium guajava* leaf extract: An eco-friendly and recyclable adsorbent for remediation of Cr(VI) from aqueous media. *Biophys. Chem.* **2020**, *263*, 106392, <https://doi.org/10.1016/j.bpc.2020.106392>.
21. Sharma, D.; Ledwani, L.; Mehrotra, T.; Kumar, N.; Pervaiz, N.; Kumar, R. Biosynthesis of hematite nanoparticles using *Rheum emodi* and their antimicrobial and anticancerous effects *in vitro*. *J. Photochem. Photobiol. B: Biol.* **2020**, *206*, 111841, <https://doi.org/10.1016/j.jphotobiol.2020.111841>.
22. Mbachu, C.A.; Babayemi, A.K.; Egbosiuwa, T.C.; Ike, J.I.; Ani, I.J.; Mustapha, S. Green synthesis of iron oxide nanoparticles by Taguchi design of experiment method for effective adsorption of methylene blue and methyl orange from textile wastewater. *Results Eng.* **2023**, *19*, 101198, <https://doi.org/10.1016/j.rineng.2023.101198>.
23. Jasrotia, T.; Chaudhary, S.; Kaushik, A.; Kumar, R.; Chaudhary, G. Green chemistry-assisted synthesis of biocompatible Ag, Cu, and Fe₂O₃ nanoparticles. *Mater. Today Chem.* **2020**, *15*, 100214, <https://doi.org/10.1016/j.mtchem.2019.100214>.

24. Karpagavinayagam, P.; Vedhi, C. Green synthesis of iron oxide nanoparticles using *Avicennia marina* flower extract. *Vacuum* **2019**, *160*, 286-292, <https://doi.org/10.1016/j.vacuum.2018.11.043>.
25. Freire, A.; Chung, E.; Mendoza, I.; Jaén, J.A. Green synthesis of iron oxide nanoparticles using *Caesalpinia coriaria* (Jacq.) Willd. fruits extract. *Hyperfine Interact.* **2023**, *244*, 6, <https://doi.org/10.1007/s10751-023-01817-6>.
26. El-Khawaga, A.M.; Ayman, M.; Hafez, O.; Shalaby, R.E. Photocatalytic, antimicrobial and antibiofilm activities of MgFe₂O₄ magnetic nanoparticles. *Sci. Rep.* **2024**, *14*, 12877, <https://doi.org/10.1038/s41598-024-62868-5>.
27. Abuzeayad, O.H.; El-Khawaga, A.M.; Tantawy, H.; Elsayed, M.A. An evaluation of the improved catalytic performance of rGO/GO-hybrid-nanomaterials in photocatalytic degradation and antibacterial activity processes for wastewater treatment: A review. *J. Mol. Struct.* **2023**, *1288*, 135787, <https://doi.org/10.1016/j.molstruc.2023.135787>.
28. Duan, S.; Wu, R.; Xiong, Y.-H.; Ren, H.-M.; Lei, C.; Zhao, Y.-Q.; Zhang, X.-Y.; Xu, F.-J. Multifunctional antimicrobial materials: From rational design to biomedical applications. *Prog. Mater. Sci.* **2022**, *125*, 100887, <https://doi.org/10.1016/j.pmatsci.2021.100887>.
29. Munir, T.; Mahmood, A.; Rasul, A.; Imran, M.; Fakhar-e-Alam, M. Biocompatible polymer functionalized magnetic nanoparticles for antimicrobial and anticancer activities. *Mater. Chem. Phys.* **2023**, *301*, 127677, <https://doi.org/10.1016/j.matchemphys.2023.127677>.
30. Zarandona, I.; Correia, D.M.; Moreira, J.; Costa, C.M.; Lanceros-Mendez, S.; Guerrero, P.; De la Caba, K. Magnetically responsive chitosan-pectin films incorporating Fe₃O₄ nanoparticles with enhanced antimicrobial activity. *Int. J. Biol. Macromol.* **2023**, *227*, 1070-1077, <https://doi.org/10.1016/j.ijbiomac.2022.11.286>.
31. El-Bassuony, A.A.; Gamal, W.; Abdelsalam, H. Impact of different magnetic materials added to silver-magnetite nanoparticles on the structural, magnetic and antimicrobial properties. *Eur. Phys. J. Spec. Top.* **2023**, *232*, 1339-1351, <https://doi.org/10.1140/epjs/s11734-022-00759-4>.
32. Archana, S.; Jayanna, B.; Ananda, A.; Shilpa, B.; Pandiarajan, D.; Muralidhara, H.; Kumar, K.Y. Synthesis of nickel oxide grafted graphene oxide nanocomposites-A systematic research on chemisorption of heavy metal ions and its antibacterial activity. *Environ. Nanotechnol. Monit. Manag.* **2021**, *16*, 100486, <https://doi.org/10.1016/j.enmm.2021.100486>.
33. Baranwal, J.; Barse, B.; Di Petrillo, A.; Gatto, G.; Pilia, L.; Kumar, A. Nanoparticles in Cancer Diagnosis and Treatment. *Materials* **2023**, *16*, 5354, <https://doi.org/10.3390/ma16155354>.
34. Uko, C.A.; Tijani, J.O.; Abdulkareem, S.A.; Mustapha, S.; Egbosiuba, T.C.; Muzenda, E. Adsorptive properties of MgO/WO₃ nanoadsorbent for selected heavy metals removal from indigenous dyeing wastewater. *Process Saf. Environ. Prot.* **2022**, *162*, 775-794, <https://doi.org/10.1016/j.psep.2022.04.057>.
35. Nahar, B.; Chaity, S.B.; Gafur, M.A.; Hossain, M.Z. Synthesis of spherical copper oxide nanoparticles by chemical precipitation method and investigation of their photocatalytic and antibacterial activities. *J. Nanomater.* **2023**, *2023*, 2892081, <https://doi.org/10.1155/2023/2892081>.
36. Karyab, H.; Ghasemi, M.; Ghotbinia, F.; Nazeri, N. Efficiency of chitosan nanoparticle with polyaluminum chloride in dye removal from aqueous solutions: Optimization through response surface methodology (RSM) and central composite design (CCD). *Int. J. Biol. Macromol.* **2023**, *249*, 125977, <https://doi.org/10.1016/j.ijbiomac.2023.125977>.
37. Zhang, B.-T.; Yan, Z.; Liu, Y.; Chen, Z.; Zhang, Y.; Fan, M. Nanoconfinement in advanced oxidation processes. *Crit. Rev. Environ. Sci. Technol.* **2023**, *53*, 1197-1228, <https://doi.org/10.1080/10643389.2022.2146981>.
38. Mejía, H.F.G.; Toledo-Alarcón, J.; Rodríguez, B.; Cifuentes, J.R.; Porré, F.O.; Haeger, M.P.L.; Ovalle, N.V.; Astudillo, C.L.; García, A. Direct recycling of discarded reverse osmosis membranes for domestic wastewater treatment with a focus on water reuse. *Chem. Eng. Res. Des.* **2022**, *184*, 473-487, <https://doi.org/10.1016/j.cherd.2022.06.031>.
39. Darezereshki, E.; Bakhtiari, F.; Alizadeh, M.; Ranjbar, M. Direct thermal decomposition synthesis and characterization of hematite (α -Fe₂O₃) nanoparticles. *Mater. Sci. Semicond. Process.* **2012**, *15*, 91-97, <https://doi.org/10.1016/j.mssp.2011.09.009>.
40. De Groot, F.; Grioni, M.; Fuggle, J.C.; Ghijsen, J.; Sawatzky, G.A.; Petersen, H. Oxygen 1s x-ray-absorption edges of transition-metal oxides. *Phys. Rev.* **B1989**, *40*, 5715, <https://doi.org/10.1103/PhysRevB.40.5715>.

41. Azam, A.; Ahmed, A.S.; Oves, M.; Khan, M.S.; Habib, S.S.; Memic, A. Antimicrobial activity of metal oxide nanoparticles against Gram-positive and Gram-negative bacteria: a comparative study. *Int. J. Nanomed.* **2012**, *7*, 6003-6009, <https://doi.org/10.2147/IJN.S35347>.
42. Wang, F.; Qin, X.; Meng, Y.; Guo, Z.; Yang, L.; Ming, Y. Hydrothermal synthesis and characterization of α -Fe₂O₃ nanoparticles. *Mater. Sci. Semicond. Process.* **2013**, *16*, 802-806, <https://doi.org/10.1016/j.mssp.2012.12.029>.
43. An, J.; Zhang, X.; Guo, Q.; Zhao, Y.; Wu, Z.; Li, C. Glycopolymer modified magnetic mesoporous silica nanoparticles for MR imaging and targeted drug delivery. *Colloids Surf. A: Physicochem. Eng. Asp.* **2015**, *482*, 98–108, <https://doi.org/10.1016/j.colsurfa.2015.04.035>.
44. Valášková, M.; Tokarský, J.; Pavlovský, J.; Prostějovský, T.; Kočí, K. α -Fe₂O₃ Nanoparticles/Vermiculite Clay Material: Structural, Optical and Photocatalytic Properties. *Materials* **2019**, *12*, 1880. <https://doi.org/10.3390/ma12111880>.
45. Liu, B.; Sun, S.; Zhang, M.; Ren, L.; Zhang, H. Facile synthesis of large scale and narrow particle size distribution polymer particles via control particle coagulation during one-step emulsion polymerization. *Colloids Surf. A: Physicochem. Eng. Asp.* **2015**, *484*, 81-88, <https://doi.org/10.1016/j.colsurfa.2015.07.050>.
46. Jing, Z.; Wu, S. Preparation and magnetic properties of spherical α -Fe₂O₃ nanoparticles via a non-aqueous medium. *Mater. Chem. Phys.* **2005**, *92*, 600-603, <https://doi.org/10.1016/j.matchemphys.2005.02.005>.
47. Opačak, I.; Ristić, M.; Musić, S. Preparation and characterization of hollow α -Fe₂O₃ irregular microspheres. *Mater.Lett.* **2010**, *64*, 2555-2558, <https://doi.org/10.1016/j.matchemphys.2015.11.021>.
48. Raja, K.;Jaculine, M.M.; Jose, M.; Verma, S.; Prince, A.A.M.; Ilangovan, K.; Sethusankar, K.; Das, S.J. Sol-gel synthesis and characterization of α -Fe₂O₃ nanoparticles. *Superlatt. Microstruct.* **2015**, *86*, 306-312, <https://doi.org/10.1016/j.spmi.2015.07.044>.
49. Gilbert, B.; Frandsen, C.; Maxey, E.; Sherman, D. Band-gap measurements of bulk and nanoscale hematite by soft x-ray spectroscopy. *Phys. Rev. B - Condens. Matter Mater. Phys.* **2009**, *79*, 035108, <https://doi.org/10.1103/PhysRevB.79.035108>.
50. Wen, X.; Wang, S.; Ding, Y.; Wang, Z.L.; Yang, S. Controlled growth of large-area, uniform, vertically aligned arrays of α -Fe₂O₃ nanobelts and nanowires. *J. Phys. Chem. B* **2005**, *109*, 215-220, <https://doi.org/10.1021/jp0461448>.
51. Atta-ur-Rahman; Choudhary, M.I.; Thomsen, W.J. *Bioassay Techniques for Drug Development*, 1st Edition; CRC Press: London, **2001**; <https://doi.org/10.3109/9780203304532>.

Publisher's Note & Disclaimer

The statements, opinions, and data presented in this publication are solely those of the individual author(s) and contributor(s) and do not necessarily reflect the views of the publisher and/or the editor(s). The publisher and/or the editor(s) disclaim any responsibility for the accuracy, completeness, or reliability of the content. Neither the publisher nor the editor(s) assume any legal liability for any errors, omissions, or consequences arising from the use of the information presented in this publication. Furthermore, the publisher and/or the editor(s) disclaim any liability for any injury, damage, or loss to persons or property that may result from the use of any ideas, methods, instructions, or products mentioned in the content. Readers are encouraged to independently verify any information before relying on it, and the publisher assumes no responsibility for any consequences arising from the use of materials contained in this publication.